J. Biochem. 2010;147(2):191–200 doi:10.1093/jb/mvp175

JB THE JOURNAL OF BIOCHEMISTRY

Multiple conformational state of human serum albumin around single tryptophan residue at various pH revealed by time-resolved fluorescence spectroscopy

Received July 2, 2009; accepted September 25, 2009; published online November 2, 2009

Takuhiro Otosu, Etsuko Nishimoto and Shoji Yamashita*

Institute of Biophysics, Faculty of Agriculture, Graduate School of Kyushu University, Hakozaki, Fukuoka 812-8581, Japan

*Shoji Yamashita, Institute of Biophysics, Faculty of Agriculture, Graduate School of Kyushu University, Hakozaki, Fukuoka 812-8581, Japan. Tel/Fax: +81-92-642-4425; E-mail: yamashita@brs.kyushu-u.ac.jp

Human serum albumin (HSA) plays important roles in transport of fatty acids and binding a variety of drugs and organic compounds in the circulatory system. This protein experiences several conformational transitions by the change of pH, and the resulting conformations were essential for completing the physiological roles *in vivo*. Steady-state and time-resolved fluorescence spectroscopy was applied to single tryptophan residue solely arranged in HSA to study subtle conformational change around single tryptophan residue in HSA at various pH. The results showed the characteristic feature of local conformation around tryptophan residue in domain II responding to the change in entire structure. The study of time-resolved area-normalized fluorescence emission spectra (TRANES) also showed the peculiar dielectric property of water molecule trapped nearby tryptophan residue depending on pH. These results suggested that microenvironment around tryptophan residue was tightly packed at acidic and basic pH although entire conformation was loosened.

Keyword: human serum albumin (HSA)/ANS fluorescence/time-resolved area-normalized fluorescence emission spectra (TRANES)/time-resolved fluorescence decay/time-resolved fluorescence anisotropy.

Abbreviations: ANS, 1,8-anilinonaphthalene sulfonate; HSA, human serum albumin; TRANES, time-resolve area-normalized fluorescence emission spectra.

Human serum albumin (HSA) is the most abundant human blood plasma protein, and binds and transports fatty acids, drugs and other organic compounds in the circulatory system. The extraordinary ligand binding properties of HSA was reviewed in previous reports (*1*, *2*). HSA is a single polypeptide chain consisting of 585 amino acids and is composed of three homologous domains I–III and each domain has two sub-domains, a and b. The adjunction point of sub-domain a and b of domain II occupies the central position of whole structure of HSA. Interestingly, a single tryptophan residue (W214) which is a valuable intrinsic fluorescence probe and basic and acidic amino acid residues are arranged at this region.

It has been reported that HSA adopted peculiar conformations responding to the change of pH. In neutral pH (~pH 7), HSA takes heart-shaped three-dimensional structure (Fig. 1) (*3*). This conformation is referred as a normal form (N form). First conformational transition is recognized at pH 4.3 and the conformation of HSA changes to F form when pH value is decreased from neutral pH to acidic pH. F form of HSA migrates faster than any other form on electrophoresis to suggest that HSA folds more compactly at this state. By further lowering pH <2.7, F conformation changes to E form. E form of HSA created in the extremely low pH conditions exhibits similar characteristics with one of folding/unfolding intermediate state. It maintains the loosely packed tertiary structure while the secondary structure is not so much changed. On the other side of pH, a conformational transition takes place at about pH 8.0 and the conformation of HSA changes from N form to the basic form (B form). These conformational transitions are summarized below (*4*).

Conformation transitions	E ⟷ F	⟷ N	⟷ B
pH Value	2.7	4.3	8.0

These conformational transitions are important factor in physiological and protein engineering aspect because HSA binds or releases a variety of substances including drugs during transportation in the circulatory system *in vivo* through the conformational change. This is why the multiple conformational states and the structure of HSA–ligand complex have been studied extensively (*5–11*).

Fluorescence spectroscopy is one of the most useful tools to elucidate the local conformation, subtle interaction with surrounding environment, and flexibility of segment and entire motion of protein. Above all, time-resolved fluorescence spectroscopy has widely used to the studies on important biological systems such as protein–ligand interaction, folding/unfolding mechanism of protein and channel formation (*12–16*). In the present work, local conformation state around W214 arranged at the domain II responding the pH change was investigated by the time-resolved fluorescence spectroscopy.

The fluorescence decay kinetics of protein, even if single tryptophan (Trp) containing protein is usually described by multi-exponential function, and the

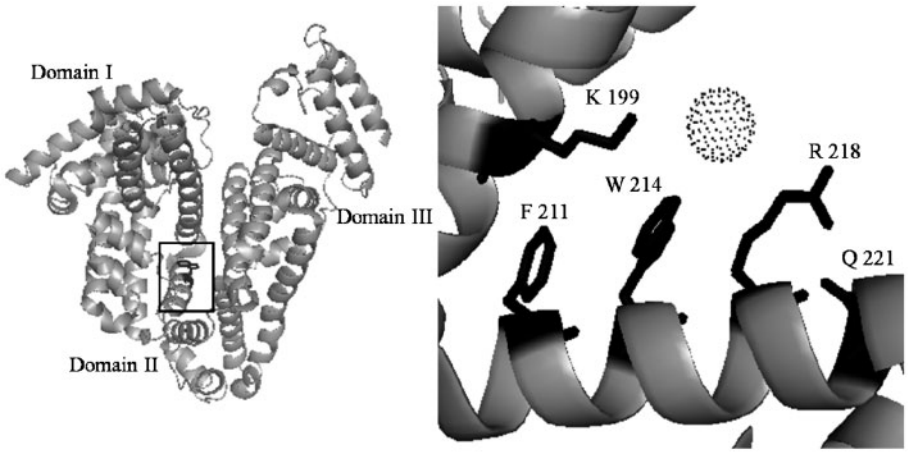

Fig. 1 X-ray crystallographic structure of human serum albumin at neutral pH. Left panel: Overall structure. Right panel: The local structure around W214. Dots sphere represents water molecule located near W214. These structures are reconstructed based on PDB, 1E78 by using PyMOL software.

photophysical relaxation mechanism and interaction with the surrounding nearby Trp residue are explained through some characteristics parameters such as decay time and corresponding amplitude. Previous studies showed that conformational heterogeneity and dielectric relaxation process on the excited state were both involved in the peculiar fluorescence decay property of Trp in protein (*17–22*). We recently studied the fluorescence decay property of indole compounds in glycerol (*23*) and confirmed that the analysis of time-resolved area-normalized fluorescence emission spectra (TRANES) is useful to assign and analyze those two kinds of kinetics from the fluorescence decay. The analytical method and application of TRANES were precisely explained by Chorvat and Chorvatova (*24*), Shaw and Pal (*25*), Koti *et al.* (*26*,*27*) and Ira *et al.* (*28*). In brief, TRANES is consistent with time-resolved peak-normalized emission spectra when dielectric relaxation of one emitting species of the chromophore is involved in the fluorescence decay, and the spectral shift rate represents the rate of energy relaxation. On the other hand, TRANES shows isoemissive point in their spectra when more than two emitting species are involved in the fluorescence decay kinetics. These characteristics of TRANES display great advantage to extract and analyze the peculiar fluorescence decay property of Trp in protein.

In this study, we have studied the local structural properties near Trp residue experienced in the multiple conformational states of HSA by steady-state, time-resolved and depolarization measurement of Trp fluorescence.

Materials and methods

Materials

HSA which is essentially fatty acid and globulin free was purchased from Sigma-Aldrich (St. Louis, MO). Other chemicals including 1-*anilino*-8-naphthalenesulfonate (ANS) were of highest grade and used without further purification. HSA was dissolved in various buffers (N form, 20 mM sodium phosphate buffer, pH 7.0; F form, 20 mM sodium acetate buffer, pH 4.1; E form, 20 mM glycine–HCl buffer, pH 2.0; B form, 20 mM glycine–NaOH buffer, pH 9.0). These protein solutions were incubated at 20°C at 6 h. In these conditions, any change of experimental parameters was not recognized after the incubation. The concentrations of HSA were spectrophotometrically adjusted to <10 μM in the buffer solution.

Steady-state fluorescence measurements

The steady-state fluorescence emission spectra were recorded on Hitachi 850 fluorescence spectrophotometer (Tokyo, Japan). The excitation wavelength was set to 295 nm in order to exclusively excite Trp in HSA. The fluorescence emission spectra were strictly corrected against detection and excitation systems. The undesired stray light were also removed by subtraction.

In ANS-binding experiment, ANS was dissolved in water (~0.3 mM) and small aliquots of the ANS solution were added to the HSA solution in a various buffer at desired pH. These protein solutions were incubated at 20°C at 30 min to attain the equilibrium. Excitation wavelength was set to 350 nm.

Time-resolved fluorescence intensity and anisotropy measurements

Time-resolved fluorescence intensity and anisotropy measurements were performed on apparatus with the subpicosecond laser based time-correlated single photon counting method (TCSPC) as described in ref. (*12–14*). An excitation pulse was generated from a combination of subpicosecond Ti:Sapphire laser (Tsunami, Spectra-Physics, MountainView, CA), pulse picker with second harmonic generator (model 3980, Spectra-Physics), and third harmonic generator (GWU, Spectra-Physics). The repetition rate was set at 800 kHz, and the full width at half-maximum (FWHM) of excitation pulse obtained was 100 fs. The stop pulse to drive the time to amplitude converter (TAC, 457, Ortec, Oak Ridge, TN) was obtained by a high speed avalanche photodiode (APD, C5658, Hamamatsu Photonics, Shizuoka, Japan). The fluorescence emission pulse worked as a start pulse of TAC was detected and amplified by a multichannel plate type photomultiplier (3809U-50, Hamamatsu Photonics) with high speed amplifier (C5594, Hamamatsu Photonics) and fast timing amplifier (FTA820, Ortec). The start and stop signals were fed into TAC through a constant fraction discriminator (CFD, 935, Ortec). The output signals of TAC were accumulated in 2048 channels in a multi-channel analyzer (Maestro-32, Ortec). The channel width was 20.43 ps/ch. The FWHM of instrument response function was 150 ps.

Fluorescence decay data analysis

The fluorescence decay kinetics were described with a linear combination of exponentials,

$$F_v(v,t) = \sum_{i=1}^{N\exp} \alpha_i(v) \exp\{-t/\tau_i(v)\}, \quad (1)$$

where v is the emission wavenumber, $F_v(v, t)$ is the spectrally- and time-resolved fluorescence decay, $\tau_i(v)$ is the wavenumber-dependent fluorescence decay time of ith component and $\alpha_i(v)$ is the corresponding pre-exponential factor. $\alpha_i(v)$ and $\tau_i(v)$ were determined by iterative convolution and non-linear curve fitting methods. Average lifetime (τ_{ave}) was expressed as follows:

$$\tau_{ave} = \frac{\sum_i \alpha_i \tau_i^2}{\sum_i \alpha_i \tau_i}. \quad (2)$$

The adequacy of curve-fitting was judged by the residual plots, the serial variance ratio (SVR) and the sigma value (*29*).

In time-resolved anisotropy measurements, a Gran–Taylor polarizer was set just behind the sample to measure the decays of vertical [$I_{vv}(t)$] and horizontal [$I_{vh}(t)$] emission components against the vertical excitation. These were related with the fluorescence decay, $F(t)$ and anisotropy decay, $r(t)$ by the following Eqs. (3) and (4),

$$I_{vv}(t) = \frac{1}{3}F(t)\{1 + 2r(t)\}, \quad (3)$$

$$I_{vh}(t) = \frac{1}{3}F(t)\{1 - r(t)\}. \quad (4)$$

The fluorescence anisotropy decay kinetics was given by Eq. (5),

$$r(t) = \sum_i \beta_i \exp(-t/\varphi_i), \quad (5)$$

where ϕ_i is the rotational correlation time of ith component and β_i is the corresponding amplitude. Their adequacies were confirmed by SVR and sigma for the decay of parallel [$I_{vv}(t)$] and perpendicular [$I_{vh}(t)$] components.

Time-resolved area-normalized fluorescence emission spectra

The time-resolved emission spectra were constructed using Eq. (*1*) as follow:

$$I(v,t) = v^{-3}F_v(v,t). \quad (6)$$

It is denoted that pre-exponential factors in Eq. (*1*) were corrected by multiplying $F_v^{SS}/\Sigma\alpha_i(v)\tau_i(v)$, where F_v^{SS} is steady-state fluorescence intensity. As for the analysis of time-resolved emission spectra, two spectra based on different normalization methods were reported, that is, peak-normalized emission spectra and TRANES. Previous study (*23*) showed that TRANES gives us more information than peak-normalized one. The most useful feature in TRANES is the appearance of isoemissive point (*25*, *26*).When fluorescence emitted from two independent species A* and B* and no dielectric relaxation process occurs in experimental time window, isoemissive point is found at v_i (cm^{-1}),

$$\frac{k_{ra}(v_i)}{k_{rb}(v_i)} = \frac{k_{ra}}{k_{rb}}, \quad (7)$$

$$k_{ra} = \int_0^\infty k_{ra}(v)dv,$$

$$k_{rb} = \int_0^\infty \int k_{rb}(v)dv, \quad (8)$$

where k_{ra} (v_i) and k_{rb} (v_i) are the radiative rates of A* and B* at v_i, respectively.

To construct TRANES from Eq. (*6*), we need to know the area value of each spectrum. Therefore, fluorescence decay data covering the entire spectral region is required, but getting those data is difficult because of its weakness of signal at around the edge of the spectrum. In this study, we fitted each time-resolved fluorescence spectrum with double Gaussian line shape equations expressed as follows to estimate the area of the spectra,

$$I(v,t) = \sum_{i=1}^{2} \frac{A_i(t)}{(\pi/2)^{1/2}w_i(t)} e^{-2((v-v_i(t))/w_i)^2}, \quad (9)$$

where $A_i(t)$ is the area, $w_i(t)$ is the FWHM and $v_i(t)$ is the center of gravity of each spectrum of ith component.

Results

Steady-state fluorescence spectroscopy of W214 in HSA at various pH

Figure 2 showed steady-state fluorescence spectra of single tryptophan residue (W214) in HSA at various pH. In N form (pH 7.0), the spectral peak wavelength was 348 nm which suggested that W214 locates hydrophilic environment and was exposed to solvent. In crystallographic structure of HSA, it seems that W214 locates at the bottom of crevice in domain IIA and packed in the protein matrix. But a trapped water was seen in Fig. 1 which would give polar environment to W214 (*3*). The fluorescence spectrum of HSA shifted to blue side (340 nm) by decreasing pH to 4.1. This suggested that W214 is surrounded by less polar microenvironment accompanying with the conformational transition N → F. The fluorescence intensity was slightly decreased by the transition indicating that the distance between W214 and some quenching elements would be shorter than that in N form. The peak wavelength shifted further to blue side (336 nm) and the fluorescence intensity was further decreased by the F → E conformational transition. These results demonstrated that the packing around W214 of E form was more enhanced than that of F form. Previous studies on the conformational changes of HSA showed that the structure of HSA expands to maximum extent in E form, and no interactions occur between domains and also between subdomains (*4*, *30*). But fluorescence data in this study suggested that microenvironment around W214 was packing tightly at low pH. On the other hand, slightly blue shift of the fluorescence spectrum was observed by increasing pH from 7.0 to 9.0, but the range of the shift was smaller than that of the transition N → F.

ANS binding to HAS

The fluorescence intensity of some dyes such as ANS are very weak in polar environment (water) but

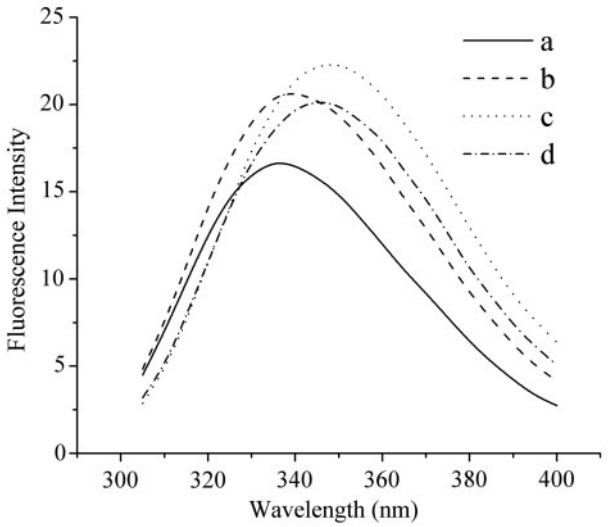

Fig. 2 Steady-state fluorescence spectra of W214 in HSA at various pH (a, pH 2.0; b, pH 4.1; c, pH 7.0; d, pH 9.0). Excitation wavelength was 295 nm.

remarkably enhanced by binding with hydrophobic sites in protein. Therefore, the fluorescence of ANS has been widely used to study the accessibility of ANS to hydrophobic sites (*31*). Figure 3 showed the fluorescence spectrum of ANS in HSA solution at various pH. At neutral and basic pH, ANS was slightly bound to HSA suggesting that the contact between ANS and hydrophobic sites was restricted in N and B forms. By lowering pH to 4.1, the fluorescence intensity of ANS was increased, and the intensity was much more increased by further lowering pH to 2.0. This result indicated that hydrophobic sites in HSA were exposed to solvent at low pH. Previous study using CD and dynamic light scattering supported the idea that the structure of HSA would loose at low pH (*30*). In the ANS binding study, the change of fluorescence intensity originated from the conformational transition N → B was not observed.

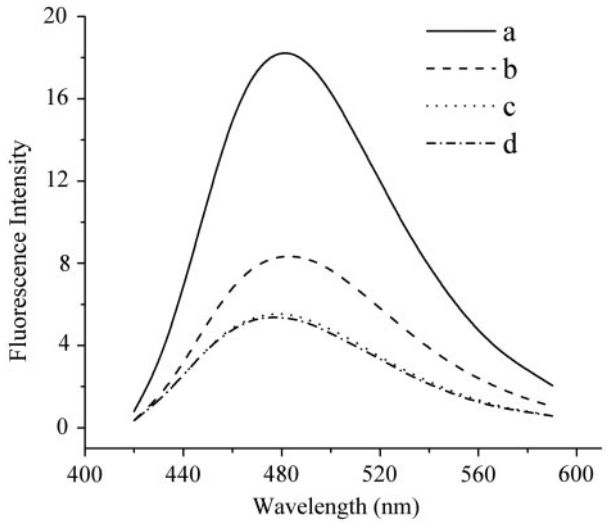

Fig. 3 Fluorescence spectra of ANS in HSA solution at various pH (a, pH 2.0; b, pH 4.1; c, pH 7.0; d, pH 9.0). Excitation wavelength was 350 nm.

Time-resolved Fluorescence of W214 in HSA at various pH

Fluorescence decay profiles of W214 in HSA at various pH were shown in Fig. 4. Representative fitting parameters giving the best fit were listed in Table 1. The fluorescence decay of W214 in every pH conditions could be best fitted by the sum of at least three exponentials. The average lifetimes (τ_{ave}) increased as increasing emission wavelength, but different amplitude is estimated dependent on pH. The measurement of fluorescence decay was performed on various emission wavelengths (315–400 nm) but no negative amplitude was recognized.

By using the fluorescence decay parameters, TRANES were constructed in two different time regions. Figures 5 and 6 showed TRANES of W214 in HSA at various pH conditions in 0.1–3.6 and 4.4–12 ns regions, respectively.

The shape of TRANES in 0.1–3.6 ns time regions represented different spectral shift pattern dependent on pH. At pH 2.0 and 9.0, isoemissive point was seen in TRANES (Fig. 5A and D). The appearance of isoemissive point in TRANES suggested the involvement of two different emission species on the fluorescence decay in this time region. In the same pH conditions, the other isoemissive point in TRANES appears in Fig. 6A and D in 4.4–12 ns time region. These two isoemissive points appeared in different time regions suggested that three emission species of W214 which

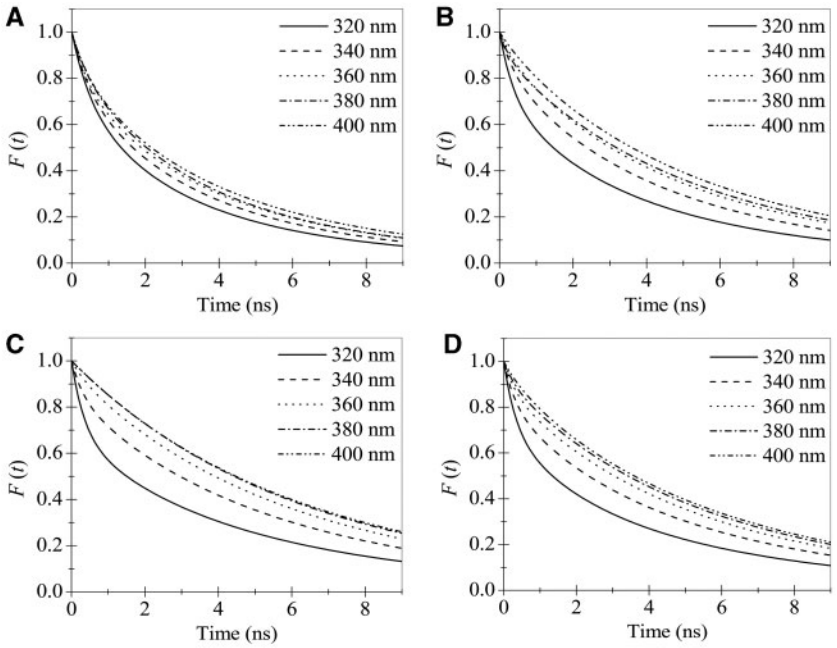

Fig. 4 Fluorescence decay profiles of W214 in HSA at various pH (A, pH 2.0; B, pH 4.1; C, pH 7.0; D, pH 9.0). Excitation wavelength was set to 295 nm. The decay profiles at each pH were calculated by using fluorescence decay parameters giving the best fit to the observed decay data.

Table 1. Fluorescence decay parameters of W214 in HSA at various pH values.

pH	λ (nm)	α_1	α_2	α_3	τ_1 (ns)	τ_2 (ns)	τ_3 (ns)	Sigma	SVR	τ_{ave} (ns)
2.0	320	0.39	0.37	0.24	5.27	1.96	0.47	1.02	1.84	4.26
	340	0.49	0.32	0.19	5.29	1.96	0.41	1.06	1.99	4.54
	360	0.53	0.32	0.16	5.54	2.03	0.35	1.02	1.97	4.84
	380	0.47	0.41	0.13	5.88	2.33	0.39	1.02	1.94	4.90
	400	0.59	0.28	0.12	5.71	1.96	0.39	0.99	1.93	5.13
4.1	320	0.48	0.27	0.26	5.64	1.96	0.37	0.97	1.82	4.91
	340	0.58	0.28	0.14	6.15	2.45	0.39	1.06	1.98	5.49
	360	0.67	0.26	0.07	6.42	2.66	0.42	1.03	1.95	5.87
	380	0.63	0.28	0.09	6.83	3.17	0.26	1.13	2.04	6.18
	400	0.61	0.35	0.04	7.25	3.60	0.62	1.06	2.01	6.41
7.0	320	0.50	0.19	0.31	6.58	2.16	0.35	0.98	1.82	6.00
	340	0.70	0.17	0.14	6.79	2.45	0.31	1.03	1.89	6.39
	360	0.68	0.27	0.04	7.52	3.67	0.36	1.04	1.82	6.78
	380	0.40	0.60	–	9.11	5.15	–	1.08	1.81	6.70
	400	0.80	0.20	–	7.57	3.63	–	1.04	1.88	6.93
9.0	320	0.48	0.24	0.28	6.00	1.75	0.32	1.03	1.94	5.31
	340	0.63	0.20	0.17	6.29	2.02	0.30	1.00	1.98	5.82
	360	0.67	0.22	0.11	6.70	2.84	0.32	1.02	1.99	6.18
	380	0.64	0.28	0.08	7.07	3.41	0.31	1.06	2.05	6.42
	400	0.80	0.16	0.05	6.67	2.36	0.40	1.06	1.97	6.37

Excitation wavelength, 295 nm. The fluorescence lifetimes (τ_i) and corresponding amplitudes (α_i) were calculated by fitting experimental fluorescence decay data by Eq. (1). Average lifetime (τ_{ave}) was calculated by Eq. (2).

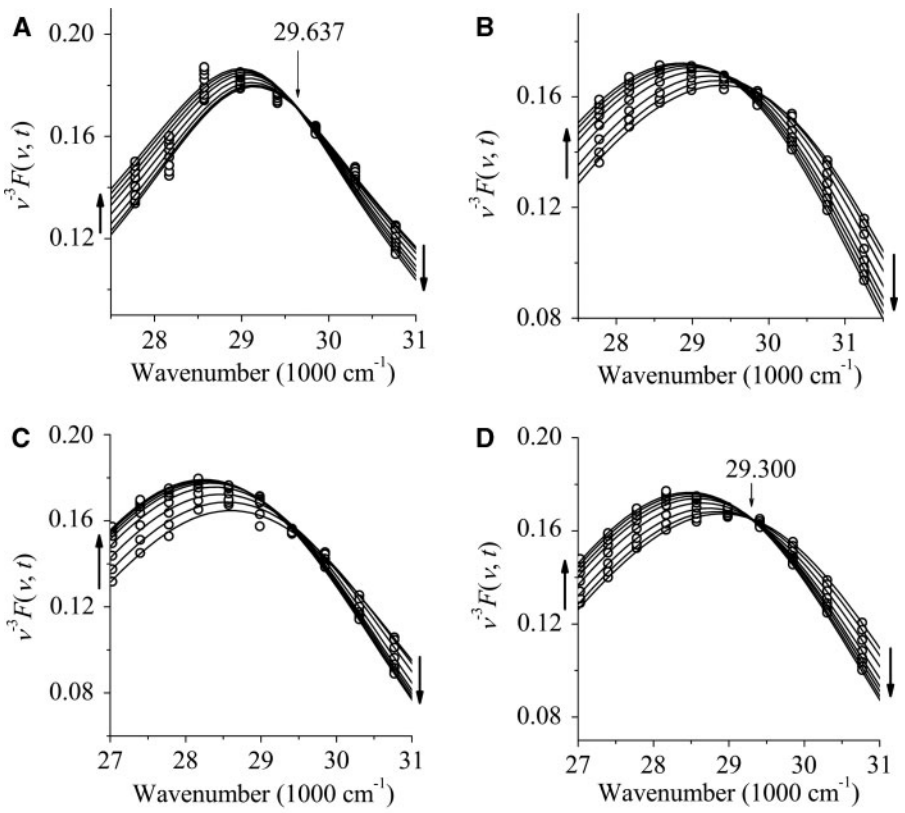

Fig. 5 Time-resolved area-normalized fluorescence spectra of HSA at various pH (A, pH 2.0; B, pH 4.1; C, pH 7.0; D, pH 9.0) in 0.1–3.6 ns time region. The data at each pH were fitted by double-Gaussian equation to estimate the area of each spectrum shown in solid lines. Thin arrows and values in A and D, represent the isoemissive points and corresponding wavenumbers, respectively, and thick arrows in all figures represent the time evolution of spectral shift.

have inherent fluorescence lifetimes and energy differences between excited- and ground-state exist in HSA. It is also suggested that the dielectric relaxation process against excited state dipole moment of W214 in HSA would be surpressed at pH 2.0 and 9.0 in two time regions. Therefore, fluorescence decay properties of W214 in HSA at these pH are explained by rotamer/conformer model. Each decay component and their

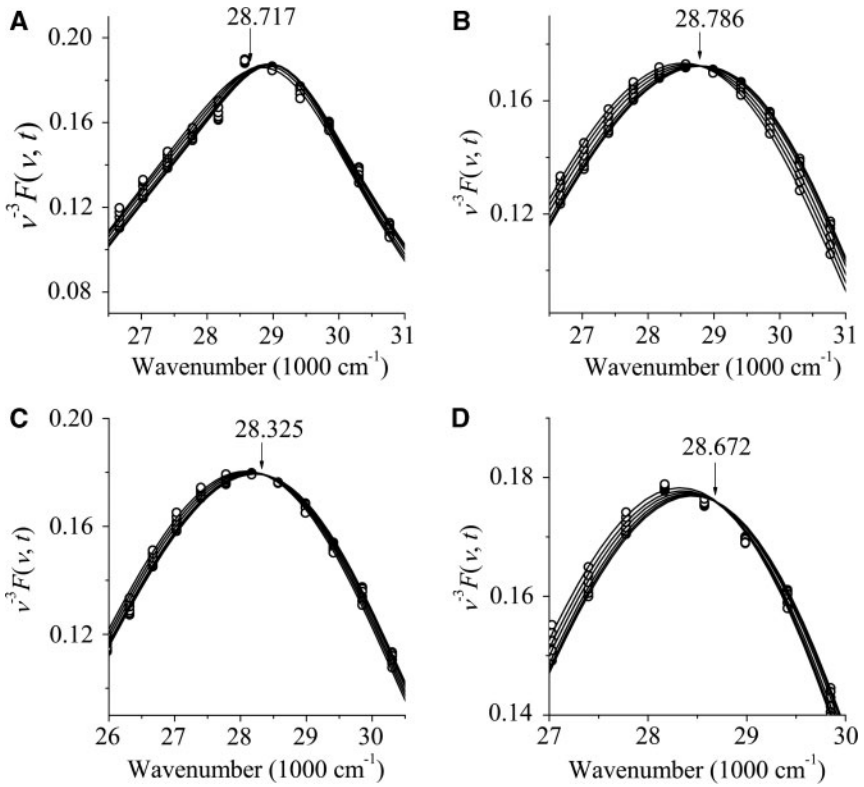

Fig. 6 Time-resolved area-normalized fluorescence spectra of HSA at various. pH (A, pH 2.0; B, pH 4.1; C, pH 7.0; D, pH 9.0) in 4.4–12 ns time region. The data at each pH were fitted by double-Gaussian equation to estimate the area of each spectrum shown in solid lines. Thin arrows and values represent the isoemissive points and corresponding wavenumbers, respectively.

amplitudes shown in Table 1 reflected the fluorescence lifetime of each rotamer/conformer and these contributions against total fluorescence, respectively.

On the contrary, isoemissive point was not found in TRANES of 0.1–3.6 ns time region at pH 4.1 and 7.0 (Fig. 5B and C) though spectral shapes of TRANES in these conditions were resemble to that at pH 9.0. If the dielectric relaxation process dominates fluorescence property, the spectral shape of TRANES must be the same as peak-normalized time-resolved fluorescence emission spectra. Therefore, the present result suggested that both dielectric relaxation and conformational heterogeneity were simultaneously involved in the fluorescence property of W214 in HSA at these pH in this time region. It was generally confirmed that the appearance of negative pre-exponential factor in the fitting parameter at red side of emission wavelength represent the existence of energy relaxation process on the excited state. In this study, no such pre-exponential factor was shown in the fluorescence decay of HSA. It would be because that the negative amplitude attributed to the excited-state kinetics is counteracted by the fluorescence decay component which has the same lifetime as energy relaxation time. The previous study was also mentioned in this regard (*22*). Therefore, the lack of a fluorescence decay component having negative pre-exponential is not evidence for the absence of excited-state kinetics.

In TRANES of 4.4–12 ns time region, clear isoemissive point was found at pH 4.1 and 7.0 (Fig. 6B and C). From the data of TRANES in different time regions, it is concluded that there are three emitting species existed and involved in the fluorescence property of W214, and dielectric relaxation process which is completed within 4 ns occur in these conditions.

Fluorescence anisotropy decay of W214 in HSA at various pH

The study of fluorescence anisotropy decay of tryptophan residue can give us information about segmental flexibility and overall motion of the protein. Figure 7 showed the fluorescence anisotropy decay profiles of W214 in HSA at various pH. These data could be fitted by a sum of two exponentials. The fitting parameters giving best fit were shown in Table 2. The shorter rotational correlation time (ϕ_1) was in the order of subnanosecond in all cases which reflected the segmental motion of peptide element including W214 in HSA. On the other hand, the longer rotational correlation time (ϕ_2) reached to several tens of nanoseconds. This correlation time corresponds to the overall rotation of HSA.

Experimentally decided parameters by fitting anisotropy decay curves with Eq. (*5*) can be rearranged to Eq. (*10*) using the rotational freedom, the rotational correlation times for the tryptophyl segment and the entire motion of HSA,

$$r(t) = r_0\{f\exp(-t/\varphi_f) + (1-f)\}\exp(-t/\varphi_p). \qquad (10)$$

The rotational correlation time of peptide element including tryptophan residue (ϕ_f), the entire rotational

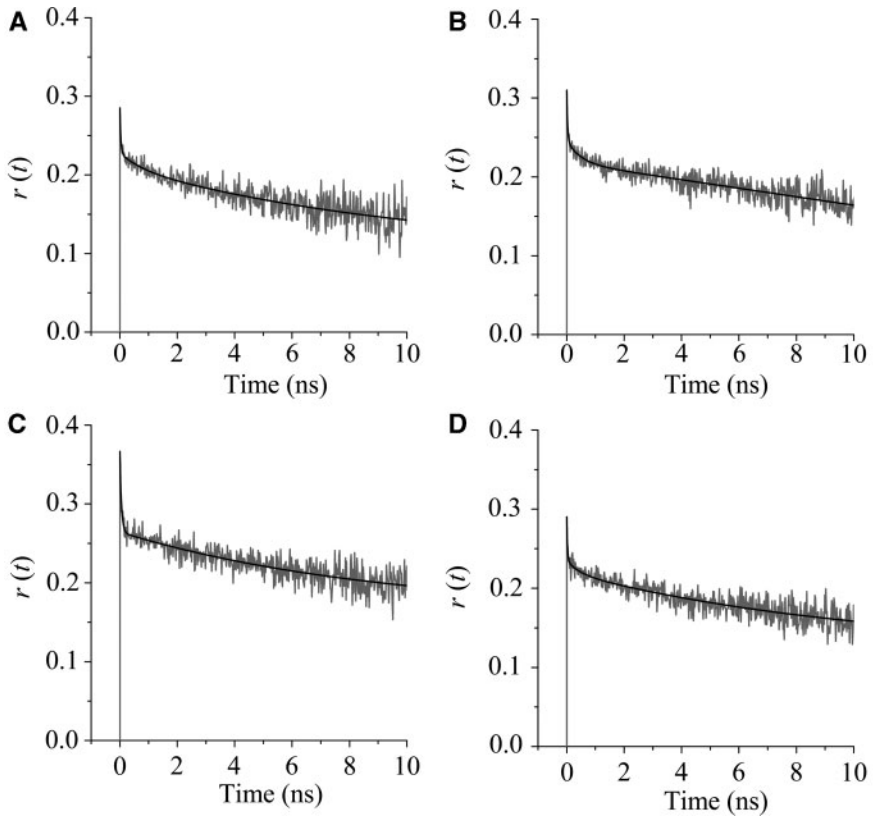

Fig. 7 Fluorescence anisotropy decay of W214 in HSA at various pH (A, pH. 2.0; B, pH 4.0; C, pH 7.0; D, pH 9.0). Excitation wavelength, 295 nm; emission. wavelength, 360 nm.

Table 2. Fluorescence depolarization parameters of HSA.

pH	β_1	β_2	ϕ_1 (ns)	ϕ_2 (ns)	sigma	SVR (VV)	SVR (VH)	f	θ
2.0	0.05	0.21	0.18	22.70	1.15	1.54	1.69	0.19	21.28
4.1	0.06	0.22	0.13	33.10	1.02	1.82	1.95	0.22	23.08
7.0	0.09	0.26	0.08	34.90	1.03	1.81	1.85	0.26	25.35
9.0	0.04	0.22	0.27	31.60	1.09	1.63	1.80	0.16	19.39

Excitation wavelength, 295 nm. Emission wavelength, 350 nm. The rotational correlation time (ϕ_i) and corresponding amplitudes (β_i) were calculated by fitting experimental fluorescence anisotropy decay data by Eq. (5). The rotational freedom (f) and the semi-cone angle for segmental motion (θ) were calculated by Eqs. (11) and (13), respectively.

correlation time (ϕ_p) and the rotational freedom (f) are related with the experimentally decided β_1, β_2, ϕ_1 and ϕ_2 as follow:

$$\frac{1}{\varphi_f}+\frac{1}{\varphi_p}=\frac{1}{\varphi_1}, \qquad \phi_p=\phi_2, \qquad f=\frac{\beta_1}{\beta_1+\beta_2}. \quad (11)$$

and r_0 is the anisotropy value at $t=0$. The experimentally decided rotational correlation times (ϕ_p) at pH 7.0 shown in Table 2 were almost coincident with the values calculated by Eq. (*12*) assuming the specific volume of the protein (v), hydration (h) and the viscosity (η) as 0.75 (ml/g), 0.4 and 1.00 (cP), respectively.

$$\varphi_p=\frac{\eta M}{RT}(v+h), \quad (12)$$

where M is the molecular weight of the protein. By using the rotational freedom, the semi-cone angle (θ) for segmental motion was calculated based on the following euqation:

$$(1-f)^{1/2}=\frac{1}{2}\cos\theta(\cos\theta+1). \quad (13)$$

The calculated semi-cone angels were also shown in Table 2.

On the conformational transition N → F, the correlation time for the segmental motion was increased and the motional freedom of W214 was decreased though overall motion was not so changed. It was suggested that the interaction of W214 with microenvironment surrounding W214 was enhanced by the transition without changing the overall spherical structure. The interaction was more strengthened on F → E transition where the rotational correlation time of peptide element including tryptophan residue was further increased and the segmental motion was

more restricted. These results were coincident with the structural property obtained by the steady-state fluorescence study of W214. The conformation surrounding W214 was packed more tightly by decreasing pH. The entire correlation time was decreased by the F → E transition. At first glance, this result would be inconsistent with the previous study that the structure of HSA expands to maximum extent (*4*, *30*). This discrepancy would be due to the fact that the structure of HSA was no more spherical at pH 2.0 and the longer correlation time (ϕ_2) would indicate the rotation along different rotational axis from that obtained at the other pH.

The similar change of microenvironment around W214 was induced on the conformational transition from neutral form (pH 7.0) to basic form (pH 9.0). In the B conformation, the shorter rotational correlation time was estimated to be 270 ps and corresponding rotational freedom was more suppressed suggesting more compact conformation formed around W214 than N form.

Discussions

In the present study, steady-state and time-resolved fluorescence study of tryptophan residue (W214) and steady-state ANS fluorescence study were attempted to characterize the multiple conformational states of HSA at various pH. The overall conformational changes of HSA were deduced from the data of ANS fluorescence and the rotational correlation time in time-resolved anisotropy decay, and the local conformations around W214 were described by steady-state spectrum, intensity and anisotropy decay analysis of tryptophan fluorescence. The results in this study showed the different characteristics between entire conformation and local one around W214 in domain II. Time-resolved fluorescence decay data showed that there are three rotamer/conformer of W214 in HSA and the lifetime of each component was similar in all conformations indicating the drastic conformational change would not occur around W214 throughout the investigated pH. In such case, it is interesting to discuss the fluorescence data measured in this study based on the crystallographic structure of HSA.

On the N → F conformational transition, fluorescence intensity of ANS was increased indicating the packing of hydrophobic site of HSA was loosened. On the other hand, the correlation time for the segmental motion and the motional freedom of W214 were prolonged and decreased by the transition suggesting peptide element around W214 was packed more compactly. By further decreasing pH to 2.0, ANS fluorescence intensity was enhanced more than three times than that in N form. Shaw *et al.* (*30*) suggested the structure of HSA loosens and expands to maximum extent at this pH which is consistent with the data of ANS-binding experiment. However, the interesting structural property was recognized in the local conformation around W214. The data of steady-state fluorescence, time-resolved fluorescence anisotropy decay showed that W214 was packed tightly in protein matrix and the interaction of W214 with surrounding molecule became strengthened at this conformation.

In TRANES analysis, the involvement of dielectric relaxation process in the fluorescence decay was detected at pH 7.0 and 4.1. In protein matrix, it is thought that trapped water drive the dipole-dipole interaction with Trp. Actually, the trapped water molecule can be found near W214 in the crystallographic structure of neutral form of HSA (Fig. 1). Therefore, dielectric relaxation processes found at these pHs demonstrates that the reorientation of trapped water molecule would be allowed near W214. There are two amino acid residues arranged near W214 in domain II of HSA. These two amino acids, K199 and R218 would give the determinant effect on the local conformation near W214 through their amino and guanidinium groups. As shown in Fig. 1, R218 locates near trapped water molecule, but the amino group in R218 orients toward amide group of Q221 at neutral and basic pH. That is why the water molecule can move and reorient, and dipole–dipole relaxation would occur in these conformations at pH 7.0 and 4.1. It was found that the motion of trapped water was suppressed at pH 2.0 and 9.0 from the results in TRANES. Human methemalbumin maintain almost same crystallographic structure to HSA and shows the similar fluorescence spectrum with HSA at pH 2.0. Therefore, the local structure around its Trp residue of methemalbumin would be interesting. No water molecule is found around Trp residue in methemalbumin (*32*). If water molecule is not arranged near W214 of HSA at pH 2.0 similarly with methemalbumin, the results obtained at pH 2.0 could be rationalized well, because, then, the polarity in the environment surrounding W214 would be lower and the tight hydrophobic interaction between the peptide elements would inhibit the rotational motion of W214. Now, the detailed crystallographic structure of HSA at extreme acid condition is not available as far as we know. Therefore, definitive discussion would be impossible. The peculiar properties in energy and motional relaxation of W214 observe at pH 2.0 might be rationalized by the interaction of the participated water molecule with the protonated K199 and R218. Their protonated amino and guanidinium group would be able to suppress the orientation of the water molecule to prohibit the dielectric relaxation through the hydrogen bond with the water molecule.

K199 and R218 may associate with the fluorescence behavior of HSA observed at pH 9.0. But in this pH condition, the peak wavelength in the fluorescence spectrum was longer than that at pH 2.0. It was suggested that W214 in HSA at pH 9.0 had different hydration properties from that at pH 2.0. The pK_a of side chain of lysine and arginine in water is larger than 9.0. However, pK_a value is sensitive to surrounding environment such as polarity. In fact, Dwyer *et al.* reported that lysine residue buried in a hydrophobic pocket in the interior of staphylococcal nuclease titrated with pK_a values of 5.8 (*33*–*36*). The protonated amino and guanidinium would give W214 a specific hydration state that the dielectric relaxation and the rotational motion of W214 occur.

HSA adopts specific forms, E, F, N and B form depending on pH conditions. The local conformation around W214 was concomitantly changed responding pH. The corresponding conformation revealed by the dielectric relaxation and rotational dynamics would be brought about the hydration and/or peculiar arrangement of basic amino acids near W214.

Conclusions

In this study, steady-state and time-resolved fluorescence spectroscopy were applied to examine the multiple conformation state of HSA at various pH. In time-resolved fluorescence study, TRANES methods were applied to the analysis of fluorescence decay property of W214 in HSA. The data suggested that the conformational transition of microenvironment around W214 in domain II was different from that of overall structure of HSA. Previous studies (*4*, *30*) and ANS experiment in this study showed the loosening of overall structure at low pH. Therefore, the conformation around W214 at low pH would contribute to the stability of overall structure of HSA at low pH.

Conflict of interest
None declared.

References

1. Fasano, M., Curry, S., Terreno, E., Galluano, M., Fanali, G. *et al*. (2005) The extraordinary ligand binding properties of human serum albumin. *IUBMB Life* **57**, 787–796
2. Peters, T. Jr. (1996) *All about Albumin, Biochemistry, Genetics, and Medical Applications*. Academic Press, New York
3. Bhattacharya, A.A., Curry, S., and Franks, N.P. (2000) Binding of the general anesthetics propofol and halothane to human serum albumin. High resolution crystal structures. *J. Biol. Chem.* **275**, 38731–38738
4. Qiu, W., Zhang, L., Okobiah, O., Yang, Y., Wang, L., and Zhong, D. (2006) Ultrafast solvation dynamics of human serum albumin: correlations with conformational transitions and site-selected recognition. *J. Phys. Chem. B.* **110**, 10540–10549
5. Roseneor, V. M., Oratz, M., and Rothschild, M.A. (1977) *Albumin Structure, Function and Uses*. Pergamon, Oxford, UK
6. Muzammil, S., Kumar, Y., and Tayyab, S. (2000) Anion-induced refolding of human serum albumin under low pH conditions. *Biochim. Biophys. Acta* **1476**, 139–148
7. Muzammil, S., Kumar, Y., and Tayyab, S. (2000) Anion-induced stabilization of human serum albumin prevents the formation of intermediate during urea denaturation. *Protein Struct. Funct. Genet.* **40**, 29–38
8. Muzammil, S., Kumar, Y., and Tayyab, S. (1999) Molten globule-like state of human serum albumin at low pH. *Eur. J. Biochem.* **266**, 26–32
9. Dockal, M., Carter, D.C., and Rüker, F. (2000) Conformational transitions of the three recombinant domeins of human serum albumin depending on pH. *J. Biol. Chem.* **275**, 3042–3050
10. Shaw, A.K. and Pal, S.K. (2008) Spectroscopic studies on the effect of temperature on pH-induced folded states of human serum albumin. *J. Photochem. Photobiol. B* **90**, 69–77
11. Patel, S. and Datta, A. (2007) Steady state and time-resolved fluorescence investigation of the specific binding of two chlorin derivatives with human serum albumin. *J. Phys. Chem. B* **111**, 10557–10562
12. Fukunaga, Y., Nishimoto, E., Yamashita, K., Otosu, T., and Yamashita, S. (2007) The partially unfolded state of β-momorcharin characterized with steady-state and time-resolved fluorescence studies. *J. Biochem.* **141**, 9–18
13. Fukunaga, Y., Nishimoto, E., Otosu, T., Murakami, Y., and Yamashita, S. (2008) The unfolding of α-momorcharin proceeds through the compact folded intermediate. *J. Biochem.* **144**, 457–466
14. Otosu, T., Nishimoto, E., and Yamashita, S. (2007) Spectrally and time-resolved fluorescence spectroscopic study on melittin-calmodulin interaction. *J. Biochem.* **142**, 655–661
15. Neyroz, P., Zambelli, B., and Ciurli, S. (2006) Intrinsically disordered structure of *Bacillus pasteurii* UreG as revealed by steady-state and time-resolved fluorescence spectroscopy. *Biochemistry* **45**, 8918–8930
16. Lee, S., Kiyota, T., Kunitake, T., Matsumoto, E., Yamashita, S., Anzai, K., and Sugihara, G. (1997) De novo design, synthesis, and characterization of a pore-forming small globular protein and its insertion into lipid bilayers. *Biochemistry*. **36**, 3782–3791
17. Hellings, M., Maeyer, M. D., Verheyden, S., Hao, Q., Damme, E. J. M. V., Peumans, W. J., and Engelborghs, Y. (2003) The dead-end elimination method, tryptophan rotamers, and fluorescence lifetimes. *Biophys. J.* **85**, 1894–1902
18. Pan, C.P. and Barkley, M.D. (2004) Conformational effects on tryptophan fluorescence in cyclic hexapeptides. *Biophys. J.* **86**, 3828–3835
19. Harvey, B., Bell, E., and Brancaleon, L. (2007) A tryptophan rotamer located in a polar environment probes pH-dependent conformational changes in bovine β-lactoglobulin A. *J. Phys. Chem. B* **111**, 2610–2620
20. Toptygin, D., Savtchenko, R.S., Meadow, N.D., and Brand, L. (2001) Homogeneous spectrally- and time-resolved fluorescence emission from single-tryptophan mutants of IIA^{Glc} protein. *J. Phys. Chem. B* **105**, 2043–2055
21. Toptygin, D., Gronenborn, A.M., and Brand, L. (2006) Nanosecond relaxation dynamics of protein GB1 identified by the time-dependent red shift in the fluorescence of tryptophan and 5-fluorotryptophan. *J. Phys. Chem. B* **110**, 26292–26302
22. Buzády, A., Erostyák, J., and Somogyi, B. (2000) Phase-fluorimetry study on dielectric relaxation of human serum albumin. *Biophys. Chem.* **88**, 153–163
23. Otosu, T., Nishimoto, E., and Yamashita, S. (2009) Fluorescence decay characteristics of indole compounds revealed by time-resolved area-normalized emission spectroscopy. *J. Phys. Chem. A* **113**, 2847–2853
24. Chorvat, D. Jr. and Chorvatova, A. (2006) Spectrally resolved time-correlated single photon counting: a novel approach for characterization of endogenous fluorescence in isolated cardiac myocytes. *Eur. Biophys. J.* **36**, 73–83
25. Shaw, A.K. and Pal, S.K. (2007) Fluorescence relaxation dynamics of acridine orange in nanosized micellar systems and DNA. *J. Phys. Chem. B* **111**, 4189–4199
26. Koti, A.S.R., Krishna, M.M.G., and Periasamy, N. (2001) Time-resolved area-normalized emission spectroscopy (TRANES): a novel method for confirming emission from two excited states. *J. Phys. Chem. A* **105**, 1767–1771

27. Koti, A.S.R. and Periasamy, N. (2001) Application of time resolved area normalized emission spectroscopy to multicomponent systems. *J. Chem. Phys.* **115**, 7094–7099
28. Ira, Koti, A.S.R., Krishnamoorthy, G., and Periasamy, N. (2003) TRANES spectra of fluorescence probes in lipid bilayers membranes: an assessment of population heterogeneity and dynamics. *J. Fluores.* **13**, 95–103
29. McKinnon, A.E., Szabo, A.G., and Miller, D.R. (1977) The deconvolution of photoluminescence data. *J. Phys. Chem.* **81**, 1564–1570
30. Shaw, A.K. and Pal, S.K. (2008) Resonance energy transfer and ligand binding studies on pH-induced folded states of human serum albumin. *J. Photochem. Photobiol. B* **90**, 187–197
31. Lakowicz, J.R. (1999) *Principles of Fluorescence Spectroscopy*., Kluwer/Academic Plenum, New York
32. Wardell, M., Wang, Z., Ho, J.X., Robert, J., Ruker, F., Ruble, J., and Carter, D.C. (2002) The atomic structure of human methemalbumin at 1.9 Å. *Biochem. Biophys. Res. Comm.* **291**, 813–819
33. Huyghues-Despointes, B.M.P., Thyrlkill, R.L., Daily, M.D., Schell, D., Briggs, J.M., Antosiewicz, J.M., Pace, C.N., and Scholtz, J.M. (2003) p*K* values of histidine residues in ribonuclease Sa: effect of salt and net charge. *J. Mol. Biol.* **325**, 1093–1105
34. Andr, I., Linse, S., and Mulder, F.A.A. (2007) Residue-specific p*K* determination of lysine and arginine side chains by indirect N and C NMR spectroscopy: application to *apo* calmodulin. *J. Am. Chem. Soc.* **129**, 15805–15813
35. Fitch, C.A., Karp, D.A., Lee, K.K., Stites, W.E., Lattman, E.E., and García-Moreno, E.B. (2002) Experimental pKa values of buried residues: analysis with continuum methods and role of water penetration. *Biophys. J.* **82**, 3289–3304
36. Dwyer, J.J., Gittis, A., Karp, D.A., Lattman, E.E., Spencer, D.S., Stites, W.E., and García-Moreno, E.B. (2000) High apparent dielectric constants in the interior of a protein reflect water penetration. *Biophys. J.* **79**, 1610–1620